Probing guided modes in a monolayer colloidal crystal on a flat metal film

Sergei G. Romanov*
Institute of Optics, Information and Photonics, University of Erlangen-Nuremberg, Haberstr. 9a, 91058, Erlangen, Germany and Ioffe Physical Technical Institute, Polythekhnicheskaya st. 26, 194021, St. Petersburg, Russia

Nicolas Vogel, Karina Bley, Katharina Landfester, and Clemens K. Weiss
Max Planck Institute for Polymer Research, Ackermannweg 10, 55128 Mainz, Germany

Sergej Orlov
Max Planck Institute for the Science of Light, Günther-Scharowsky-Str. 1, 91058 Erlangen, Germany

Alexander V. Korovin
Lashkarev Institute of Semiconductor Physics NAS, pr. Nauki 41, Kiev, 03028, Ukraine

Gennady P. Chuiko
Petro Mohyla Black Sea State University, 68 Desantnikov Str., 10, Mykolayiv, 54003, Ukraine

Alois Regensburger, Alexandra S. Romanova, Arian Kriesch, and Ulf Peschel
Institute of Optics, Information and Photonics, University of Erlangen-Nuremberg, Haberstr. 9a, 91058, Erlangen, Germany
(Received 5 October 2011; revised manuscript received 16 October 2012; published 30 November 2012)

Two-dimensional slab hybrid metal-dielectric photonic crystals, which are prepared by assembling polymer colloidal spheres into closely packed monolayers of hexagonal symmetry on a gold-coated glass substrate, show an improved confinement of light compared with a colloidal monolayer on a glass substrate. We demonstrated that the optical response of such hybrid crystals consists of diffractively coupled waveguiding modes, Fabry–Perot resonances, and Mie resonances. Correspondingly, two major mechanisms, namely, band transport and hopping of localized excitations, participate in the in-plane light transport in such hybrid crystals.

DOI: 10.1103/PhysRevB.86.195145 PACS number(s): 42.70.Qs, 73.20.Mf, 78.67.Pt

I. INTRODUCTION

Design of functional architectures for programmed processing of light flow is one of the major goals of contemporary information communication technologies. In particular, this aim can be achieved by building up the photonic energy band structure (PBG) with the help of photonic crystals (PhCs) that exploit interference of incident and scattered light.[1]

Consider the array of scatterers, which can be called photonic atoms. If identical photonic atoms are assembled in a crystal, then according to the tight binding approximation, a PBG structure emerges from hybridization of their localized resonances.[2] The band structure of a PhC consists of eigenmodes, which carry the light coupled to a PhC. Details of such bandlike light transport depend on the crystal dimensionality, the photonic atom (or unit cell) complexity, and the contrast of refractive indices between "heavy" and "light" dielectrics in a lattice, as well as the fraction of a "heavy" dielectric material.[2]

Alternatively, photonic atoms can be assembled in a disordered array, termed the photonic glass. In this case, light propagates by hopping between resonance states of randomly coupled identical resonators.[3,4] Similarly, such individual resonance states can be found in the optical properties of lattices composed of widely spaced photonic atoms providing a high refractive index contrast.[5]

Hybridization of resonances in one- or two-dimensional (1D or 2D) lattices is incomplete, and photonic atoms can couple directly to modes of environment. As a result, the electromagnetic energy leaks outside a PhC. In practice, this means degradation of optical resonances; moreover, they progressively decay with increasing frequency because of the increasing role of scattering at lattice defects. Light leakage, in turn, depends on a dielectric contrast between PhC and its environment. This situation is analogous to the light-guiding phenomenon. Obviously, not all PhCs can be made from a high-index material and be suspended in a "light" dielectric. Hence, a metal mirror can be used as an alternative method of confining light. Because a metal-dielectric interface supports surface plasmons[6] and PhC provides a grating to couple light to plasmons, such architectures are called hybrid PhCs.

The assemblies of dissimilar PhCs are known as photonic heterocrystals.[7–9] In heterocrystals, transient light accumulates the footprints of different band structures. Since the idea of PhCs can be replicated for other than photon excitations, one can imagine the combination of a dielectric PhC with a polaritonic electromagnetic crystal[10] to make, e.g., a photonic-plasmonic crystal.[11] In such a hybrid PhC, light is coupled to Bloch modes of a dielectric crystal and surface plasmon polaritons (SPPs) of a metallic structure.

Proof of principle experiments with PhCs are often made using colloidal crystals because they are easy to obtain in large scale and good quality. Moreover, they can be assembled on a metal surface.[12] Hybrid structures were made by assembling monolayers (MLs) of closely packed colloidal microspheres on a metal-coated glass substrate

(ML-metal). In fact, this architecture is one of several realizations of hybrid plasmonic-photonic crystals, which differ in PhC dimensionality and metal film corrugation.[13–18] Remarkably, the set of resonances involved in light transport in hybrid crystals can be changed by altering the hybrid topology.[11]

To date, the optical properties of MLs on dielectric substrates are well known.[19–21] Resonances in their optical spectra correspond to eigenmodes of a 2D slab PhC with hexagonal symmetry. If the same ML is assembled on an opaque metal substrate, the resonances in reflectance spectra become sharper, and their number changes.[14–16] Based on numerical modeling, one can distinguish (i) the index-guided mode, the field of which is centered in spheres, (ii) the hybrid mode possessing field maxima both at the interface and in spheres, and (iii) the SPP mode with a field localized at the metal-ML interface.[14]

The effect of using a metal substrate is remarkable. A 10 times enhancement of the quality factor for the index-guided modes allows substantial improvement in the efficiency of light emitters embedded in spheres[16] and the sensitivity of ML-Au-based gas sensors.[15] However, the cited works lack the detailed analysis of the role of light confinement, as well as the genesis of other observed resonances. Moreover, some pronounced phenomena, namely, Fabry–Perot resonances in a ML and localized resonances of individual spheres, have been overlooked.

The aim of this paper is to develop a simple approach to explain the optical properties of ML-metal hybrids. Our interpretation of experimentally observed transmission and reflectance spectra of ML-metal-substrate samples is based on decomposition of the hybrid architecture on different functional components. First, this hybrid can be seen as a planar waveguide possessing eigenmodes. Second, a 2D lattice of spheres allows coupling of incident light to guided modes of a planar waveguide and to surface plasmon polaritons at the metal-film interfaces. Third, each sphere in a ML possesses its own Mie resonances, which produce non-dispersive resonances in the transmission and reflectance spectra. Superposition of these resonances gives rise to unusual spectra of a ML-metal hybrid. This approach allows us to infer that attaching a metal film to a ML adds the hopping in-plane light transport to the conveniently observed bandlike transport.

II. EXPERIMENTAL TECHNIQUE

The ML-Au hybrid architecture was prepared by assembling a ML of carboxylated polystyrene (PS) spheres (∼2% standard deviation) with a diameter of 1063 nm on a flat glass substrate coated with a 30-nm-thick Au film (Fig. 1). The metal film was deposited on a glass substrate under high vacuum conditions by thermal evaporation. A dispersion of colloids (8 weight %) diluted with ethanol (50 volume %) was spread at the air-water interface via a tilted glass slide at an angle 45°. A Langmuir-trough-based technique was used to compress colloids to a close-packed ML by moving the barriers slowly toward each other (10 mm/min). The densely packed ML was formed on a substrate by surface lowering transfer and after drying.[22,23] Reference samples were assembled on a bare glass substrate. The scanning electron microscope images of the ML-on-metal hybrid are shown in Fig. 1.

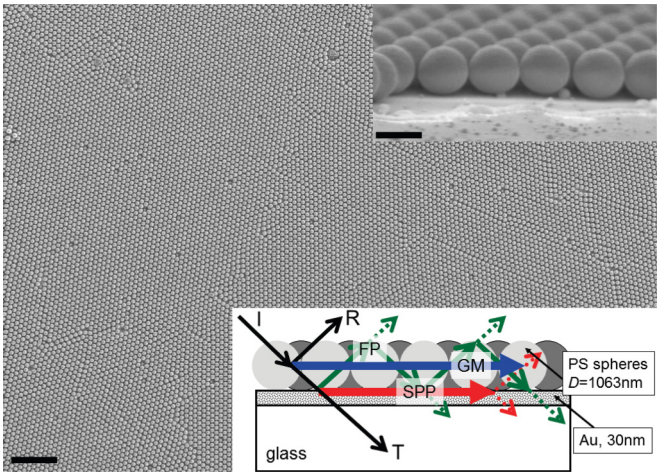

FIG. 1. (Color online) Top view, scanning electron micrograph of the ML-Au sample (scale bar = 10 μm). Inset top: this ML in a side view (scale bar = 1 μm). Inset bottom: schematic representation of waveguiding in the hybrid ML of spheres. Numbers show the dimensions of structural elements. The incidence light intensity (I) is distributed between the reflected (R), transmitted (T), and guided light. The guided light is transported by index-guided modes (GM), SPP modes, and Fabry–Perot modes (FP). Dashed arrows show light losses.

A collimated beam of white light 1 mm in diameter from a tungsten lamp was used to illuminate samples at different angles of incidence. Angular resolved transmission and reflectance spectra were acquired in *pp*- and *ss*-polarized light with 0.5° resolution in a zero-order diffraction configuration; "*pp*" and "*ss*" polarization means the light polarizer and analyzer were oriented either both parallel or both perpendicular, respectively, to the plane of light incidence. A scrambler plate in front of the spectrometer slit was used to avoid the polarization response of the spectrometer grating.

III. STRUCTURE OF OPTICAL SPECTRA

Monolayer of spheres can be considered a periodically profiled planar waveguide, the guided modes (GMs) of which are the eigenmodes of a 2D slab PhC. The transmission of this structure is high and the reflectance is low. With the aid of sphere grating, the GMs reveal themselves as minima in transmission and reflectance spectra [Fig. 2(a), curves 1, 2]. Because the refractive index (RI) of a glass substrate exceeds that of ML, the light confinement in such a waveguide is poor, and PhC eigenmodes are leaky.

It is straightforward to assume that a metal film separating a ML and substrate will improve light confinement in a ML, and dramatic changes of optical spectra shown in Fig. 2(b) support this assumption. First, transmission of the ML-Au hybrid (curve 3) is low, but reflectance (curve 4) is high. Furthermore, the number of detectable resonances is increased.

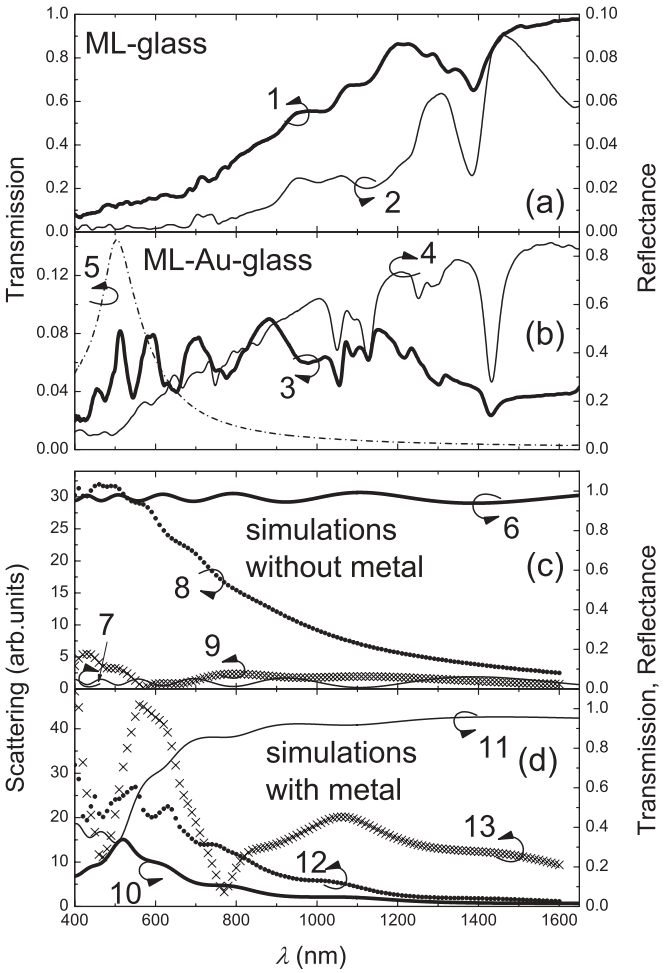

FIG. 2. Transmission (curves 1, 3) and reflectance (2, 4) spectra of (a) ML-glass sample and (b) ML-Au-glass hybrid at $\theta = 6^\circ$ in *pp*-polarized light. Curve 5 represents the transmission of 30-nm Au film. Calculated transmission (6, 10) and reflectance (7, 11) spectra of (c) 50L-glass and (d) 50L-Au-glass samples at $\theta = 0^\circ$. Calculated spectra of forward (8, 12) and backward (9, 13) scattered light of (c) sphere on a glass substrate and (d) sphere on Au-coated glass substrate at $\theta = 0^\circ$.

Early studies of reflectance spectra of ML-Au architectures based on opaque metal films revealed that long-wavelength resonances are situated at $D/\lambda \sim 0.77;\ 0.83;\ 0.89$ for normal light incidence. These resonances were assigned to SPP, dielectric, and hybrid modes, respectively.[14–16] In Fig. 2(b), the corresponding minima can be observed at 1434, 1296, and 1125 nm, but there are additional features in this sequence, with a major one at ∼1240 nm (curves 3, 4). Because these minima are observed in transmission and reflectance spectra at almost the same positions, the corresponding modes can be qualified as waveguiding.

What are the new features to note? (i) A series of strong resonances that dominate transmission at short wavelengths. (ii) Coincidence of resonance minima in transmission and reflectance spectra occurring at long wavelengths is lost at shorter wavelengths. (iii) Surprisingly, the transmission spectrum of ML-Au neglects the rapidly changing transmission of the bare Au film (Fig. 2(b), curve 5). In the following discussion, we describe this behavior with the use of different models.

IV. MULTILAYER MODEL

First, consider the eigenmodes of a waveguide, of which the dielectric permittivity profile closely resembles that of a ML of spheres. To obtain such a profile, we have to homogenize the ML. Maxwell's equations for a system with periodic permittivity, $\varepsilon(\mathbf{r}, z) = \sum_{\mathbf{G}} \varepsilon_{\mathbf{G},z} e^{i\mathbf{G}\mathbf{r}}$, where $\mathbf{r}$ is the in-plane spatial vector, $\mathbf{G}$ is the reciprocal vector, and $\varepsilon_{\mathbf{G},z}$ is the Fourier component of permittivity, can be written using the envelope function in the form $\mathbf{E}_{\mathbf{k}}(\mathbf{r}, z) = \tilde{\mathbf{E}}(\mathbf{r}, z) e^{i(\mathbf{k}\mathbf{r}-\omega t)}$,

$$(\mathbf{k}+\mathbf{G}) \times (\mathbf{k}+\mathbf{G}) \times \tilde{\mathbf{E}}_{\mathbf{G},z} = -\left(\frac{\omega}{c}\right)^2 \sum_{\mathbf{G}'} \varepsilon_{\mathbf{G}-\mathbf{G}',z} \tilde{\mathbf{E}}_{\mathbf{G}'}, \quad (1)$$

where the electric field is also a periodic function, $\tilde{\mathbf{E}}(\mathbf{r}, z) = \sum_{\mathbf{G}} \tilde{\mathbf{E}}_{\mathbf{G},z} e^{i\mathbf{G}\mathbf{r}}$.

If $|\varepsilon_{\mathbf{G}=0}| > |\varepsilon_{\mathbf{G}\neq 0}|$, the approximated solution of Eq. (1) can be found in the form

$$(\mathbf{k}+\mathbf{G}) \times (\mathbf{k}+\mathbf{G}) \times \tilde{\mathbf{E}}_{\mathbf{G},z} = -\left(\frac{\omega}{c}\right)^2 \varepsilon_{\mathbf{G}=0,z} \tilde{\mathbf{E}}_{\mathbf{G},z}, \quad (2)$$

which defines a solution for a homogeneous medium with permittivity $\varepsilon_{\mathbf{G}=0}$ and wavevector $\mathbf{k}+\mathbf{G}$. For the ML of spheres on multilayered substrate, the Fourier spectrum of the permittivity is

$$\varepsilon(\mathbf{G}, z) = \begin{cases} \varepsilon_{\text{air}}\delta(\mathbf{G}), & z > \frac{a}{2} \\ \varepsilon_{\text{air}}\delta(\mathbf{G}) + \frac{\pi}{2\sqrt{3}}(\varepsilon_{\text{sphere}} - \varepsilon_{\text{air}})(1-(2z/a)^2)\frac{2J_1(Ga\sqrt{1-(2z/a)^2})}{Ga\sqrt{1-(2z/a)^2}}, & |z| \leqslant \frac{a}{2} \\ \varepsilon_1, & d_1 < z + \frac{a}{2} \leqslant 0 \\ \cdots & \\ \varepsilon_N\delta(\mathbf{G}), & d_N < z + \frac{a}{2} + \sum_{i=1}^{N-1} d_i \leqslant 0 \end{cases}, \quad (3)$$

where, δ is the Kronecker symbol that is equal to unit for zero argument [$\delta(0) = 1$] and zero otherwise, a and ε sphere are the sphere diameter and permittivity, and d_i and ε_i are the thickness and the permittivity of layers forming multilayered substrate

correspondingly ($i = 1,2,\ldots,N$). Thus, the zero Fourier component of permittivity ($\mathbf{G} = 0$) is

$$\varepsilon(\mathbf{G}=0,\,z) = \begin{cases} \varepsilon_{\text{air}}, & z > \frac{a}{2} \\ \varepsilon_{\text{air}}\delta(\mathbf{G}) + \frac{\pi}{2\sqrt{3}}(\varepsilon_1 - \varepsilon_{\text{air}})\left(1 - \left(\frac{2z}{a}\right)^2\right), & |z| \leqslant \frac{a}{2} \\ \varepsilon_1, & d_1 < z + \frac{a}{2} \leqslant 0 \\ \ldots & \\ \varepsilon_N, & d_N < z + \frac{a}{2} + \sum_{i=1}^{N-1} d_i \leqslant 0. \end{cases} \tag{4}$$

In the following account, we will use the 50-layer (50L) approximation of this zero Fourier component profile. While guiding in this 50L structure is supported by the index profile [Fig. 3(a)], confinement is weak, and energy leaks into the substrate.

The eigenmodes of the 50L stack are shown in Figs. 3(c) and 3(d) for both polarizations. Seven modes can be found in the spectral range of interest. Due to dispersion, these modes eventually fall in the light cone, where they become familiar Fabry–Perot resonances that can be directly excited by incident light. After inserting a thin Au film between the ML and substrate (the 50L-Au structure), one can find the same seven s-polarized modes [Fig. 3(e)]. However, in p-polarized light, the number of eigenmodes is increased, since two SPP modes can be excited at interfaces of the metal film with the ML of spheres and with the substrate [Fig. 3(f)]. More than this, the dispersions of guided modes in the 50L-Au structure differ from that of the 50L structure owing to the strong frequency dependence of the dielectric permittivity of gold in the studied spectral range. In particular, at $\lambda \sim 500$ nm, the transmission of Au film peaks and reflectance dips due to interband transitions.

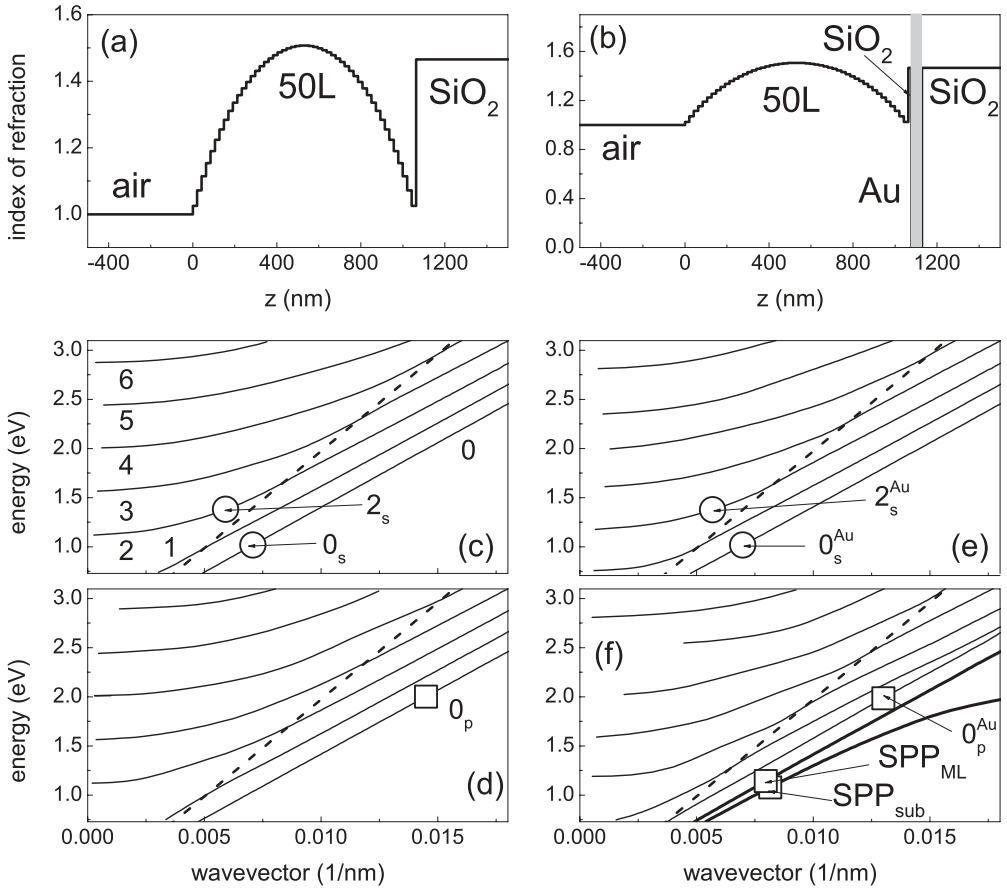

FIG. 3. Refractive index profiles of (a) 50L-glass and (d) 50L-Au-glass model structures. The complex index of gold is displayed as a grey bar. Eigenmodes of (c), (d) 50L-glass and (e), (f) 50L-Au-glass structures are shown for (c), (e) s- and (d), (f) p-polarized light, numbered consecutively. Dotted lines show the light line in air. Empty circles and squares mark the points at which the Poynting vector profiles have been calculated. Modes SPP_{ML} and SPP_{sub} in panel (f) are the SPP modes located at 50L and glass interfaces of the Au film, respectively.

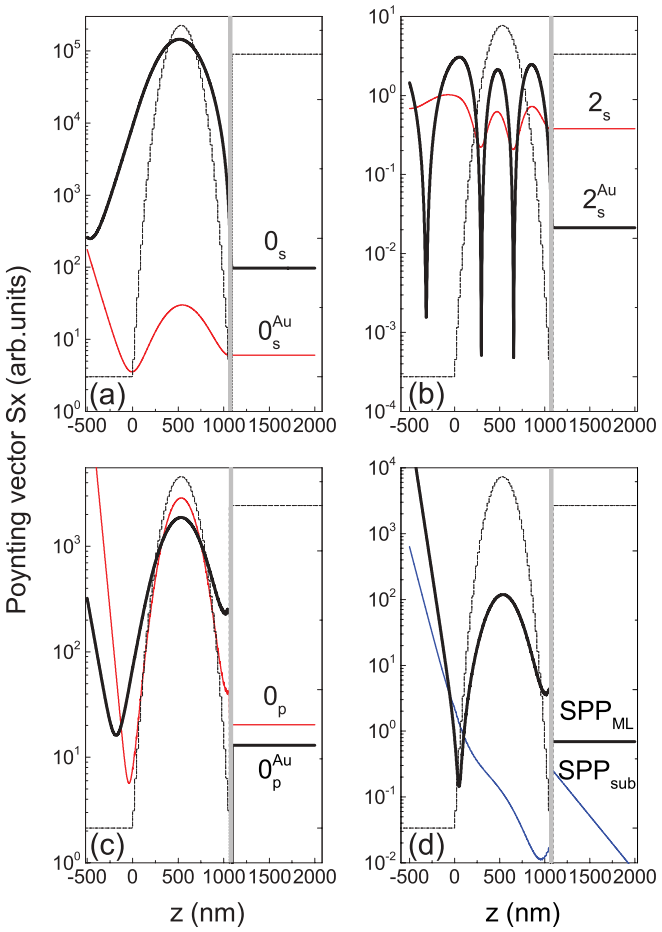

FIG. 4. (Color online) Distributions of electromagnetic flux across the 50L-glass and 50L-Au-glass structures calculated for characteristic points at dispersion curves shown in Fig. 3. Dashed lines show the refractive index profile as in Fig. 3(d). The grey bar indicates the Au film.

It is instructive to estimate the changes in light confinement introduced by a gold film. In Fig. 3, several characteristic points, for which we compared the in-plane energy flux, are indicated. Let a plane wave come from infinity and possess an electrical field of unity strength at the structure boundary $z = 0$, and let the projection of its wavevector on the slab waveguide plane $k_x^2 = (\omega/c)^2 - k_z^2$ be equal to the wavevector of an eigenmode of the 50L waveguide. If $\mathbf{k_x}$ falls in the light cone, then $\mathbf{k_z}$ is real, and the mode is radiative; otherwise, $\mathbf{k_z}$ is complex, and the eigenmode becomes evanescent.

The flux transported by the s-polarized index-guided 0_s mode in the 50L structure is concentrated at the middle of the waveguiding layer. Adding a metal mirror leads to an $\sim 10^4$ times increase of the energy coupled to the 0_s^{Au} mode [Fig. 4(a)]. For the radiative 2_s mode, one can find several nodes accommodated across the 50L structure. After adding the metal film, the energy coupled to the delocalized 2_s^{Au} mode is increased only by a factor of three [Fig. 4(b)].

The p-polarized 0_p mode remains index-guided, the flux of which is concentrated in the slab waveguide [Fig. 4(c)]. Adding a metal film changes only marginally the light flow guided by the 0_p^{Au} mode. Importantly, the $1/10$ fraction of mode power in the 50L-Au structure is bound to the ML-Au interface [i.e., the 0_p^{Au} mode acquires the character of the hybrid guided SPP mode; Fig. 4(c)].

Both $\mathrm{SPP_{ML}}$ and $\mathrm{SPP_{sub}}$ plasmon modes are evanescent [Fig. 4(d)] and are bound to opposite interfaces of the Au film. For them, the Poynting vector peaks at the metal-dielectric interface, which is a qualifying property of plasmon excitation.[24] The $\mathrm{SPP_{ML}}$ mode acquires the hybrid character because (i) the corresponding flux possesses a main maximum in the middle of a dielectric slab waveguide and (ii) the fractional maximum resides at the waveguide-metal interface. The $\mathrm{SPP_{sub}}$ mode is the only true plasmon mode, with a flux that is bound to the metal-dielectric interface. The fact that $\mathrm{SPP_{sub}}$ carries a much smaller energy compared with modes guided in a dielectric relates to the exploited excitation configuration, in which the ML acts as a gap in Kretschmann geometry.

Using transfer matrix formalism, we calculated the transmission and reflectance spectra of model planar waveguiding structures. The 50L-glass structure is highly transparent. Its spectra are modulated by Fabry–Perot oscillations so that the reflectance maximum corresponds to the transmission minimum [Fig. 2(c), curves 6, 7]. In contrast, the 50L-Au-glass structure is weakly transparent but highly reflective at $\lambda > 800$ nm [Fig. 2(d), curves 10, 11]. At shorter wavelengths, the transmission increases after transmission of the Au film [Fig. 2(b), curve 5], and the reflectance decreases toward the onset of the interband transitions in the gold, which occurs at 500 nm. However, the magnitude of Fabry–Perot oscillations remains small in both 50L-glass and 50L-Au-glass structures for incident directions close to the waveguide normal, which leaves a small chance for them to affect experimental spectra.

The Fabry–Perot oscillations of a planar waveguide are preserved in the broad range of angles of light incidence (Fig. 5). Moreover, their relative magnitude in the 50L-Au-glass structure becomes much higher for oblique light incidence compared with the 50L-glass structure. This observation points to increasing confinement of light coupled to Fabry–Perot modes along the increase in the longitudinal component of their wavevectors.

Switching between maxima and minima in p-polarized transmission of the ML-glass structure at the Brewster angle occurs due to a phase flip of reflected light [Fig. 5(b)]. This is not the case with 50L-Au-glass, for which the Brewster angle occurs at $\theta > 80^\circ$. The interband transitions in a gold film affects the spectra in the vicinity of 500 nm [Fig. 5(d)]; moreover, the spectra in p-polarized light experience stronger changes compared with s-polarized light.

V. DIFFRACTIVE COUPLING

If the ML replaces the 50L structure, the sphere grating provides diffractive light coupling to evanescent modes outside the light cone. In this case, each mode displayed in Fig. 4 expands into a series of diffraction orders, the wavevectors of which satisfy momentum conservation with vectors of the reciprocal lattice [Fig. 6(a)]. As a result, some of these diffracted orders are folded in the light cone. These modes are

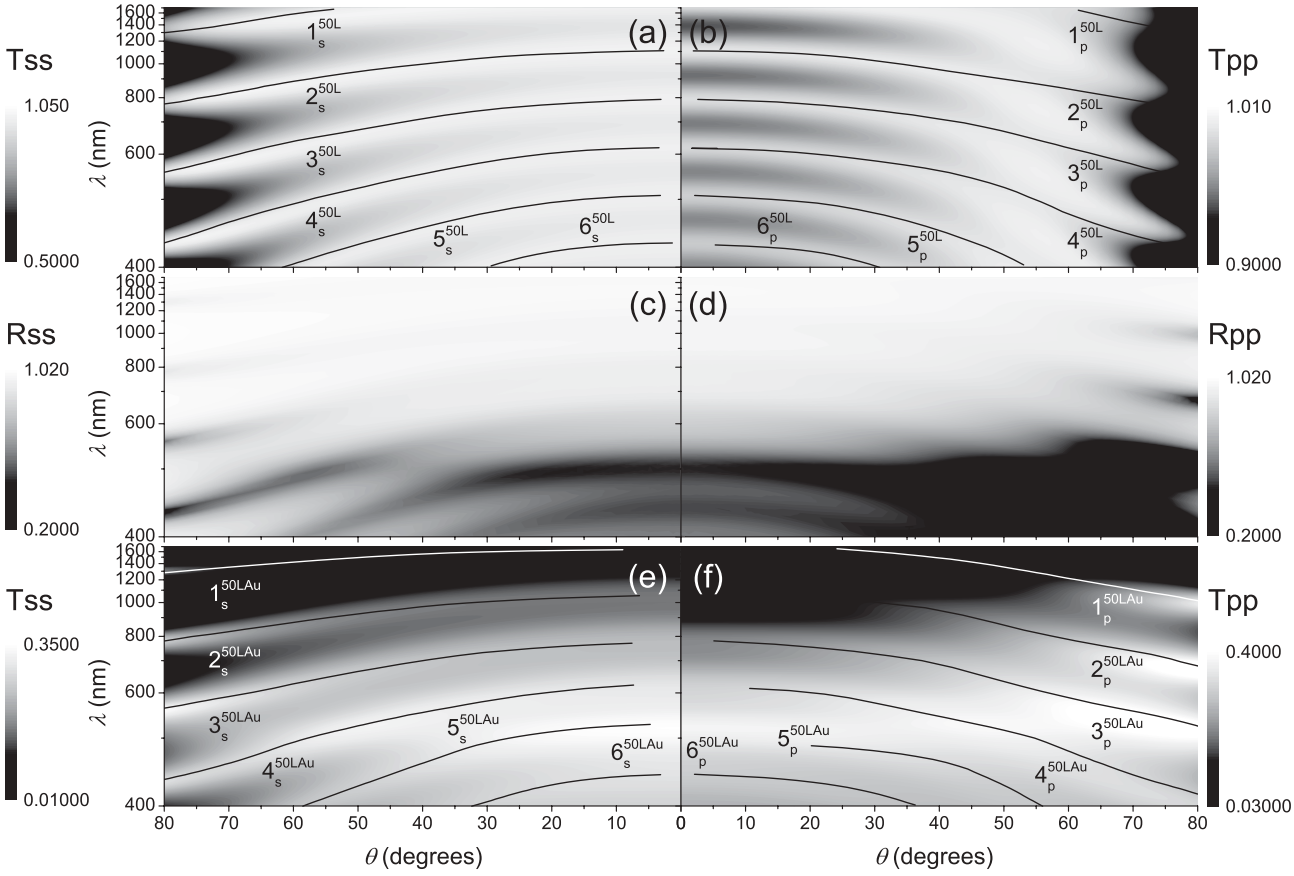

FIG. 5. (a), (b) Transmission maps of 50L-glass model. (c), (d) Reflectance and (e), (f) transmission maps of 50L-Au-glass multilayers in *s*- (left column) and *p*- (right column) polarized light.

of higher quality than Fabry–Perot oscillations because they originate from localized modes.

Since the coupling mechanism of incident light to ML-Au-glass guided modes differs from that used to calculate the Poynting vector of non-radiative modes of the 50L-Au-glass structure, the actual flux magnitude associated with quasiguided modes may change considerably. In contrast, the spatial mode localization remains the same. That is why the magnitudes of SPP_{ML}- and SPP_{sub}-related modes in experimental data appear comparable to other guided modes.

The symmetry of the hexagonal package of spheres in a ML is *p6mm*. In this group symmetry, one can find the principal sixth order rotation axis, vertical mirror reflectance plane, and two non-collinear translations of equal length with an angle of $\pi/3$ (or $\pi/6$) between them.[25] The *6mm* (C_{6v}) subgroup assumes six irreducible states in the center of the Brillouin zone: four nondegenerate 1D states (Γ_1, Γ_2, Γ_3, Γ_4) and two doubly degenerate 2D states (Γ_5, Γ_6). Hence, in a dipole approximation, one can obtain the following selection rules for optical transitions at $\mathbf{k} = 0$: (i) In *p*-polarized light ($\mathbf{e}_p || C_6$), only transitions between configurations of the same symmetry are allowed $\Gamma_n \leftrightarrow \Gamma_n$ ($n = 1, 2, 3, 4, 5, 6$); that is, modes are excited with translations that are coplanar with the plane of incidence only [Fig. 6(b)]. In this case, depending on the orientation of the $\mathbf{E}_p$ vector with respect to the lattice vector, the SPP can be excited with different efficiencies. (ii) In the *s*-polarized light ($\mathbf{e}_s \perp C_6$) only transitions between configurations of different symmetries are allowed, like

$$\Gamma_1 \leftrightarrow \Gamma_5 \leftrightarrow \Gamma_2$$
$$\updownarrow$$
$$\Gamma_3 \leftrightarrow \Gamma_6 \leftrightarrow \Gamma_4$$

[i.e., modes are only excited with translations that are non-coplanar with the plane of incidence; Fig. 6(c)]. In the latter case of the strictly transverse wave, no SPP excitation is allowed.

As a result, one can expect polarization anisotropy of diffractively coupled eigenmodes in the transmission/reflectance spectra as well as azimuthal and polarization anisotropy of the fine structure of the ML-Au spectra.

VI. MIE RESONANCES

In order to examine the nature of resonances that appear at short wavelengths, we numerically calculated the spectra of light scattered by a dielectric sphere using T-matrix formalism.[26] The electric field $\mathbf{E}_s$ scattered by a sphere on a substrate can be written as $\mathbf{E}_s = (1 - \mathbf{T}_s\mathbf{R})^{-1}\mathbf{T}_s(\mathbf{E}_p + \mathbf{E}_p^r)$, where $\mathbf{E}_p$ is an incident plane wave written on the basis of electromagnetic multipoles, $\mathbf{E}_p^r$ is a plane wave reflected by the substrate, $\mathbf{T}_s$ is a diagonal T-matrix of the sphere and $\mathbf{R}$ is a matrix, which relates the scattered-reflected field $\mathbf{E}_s^r$ with the scattered field $\mathbf{E}_s$ through $\mathbf{E}_s^r = \mathbf{R}\mathbf{E}_s$.[27] We assume

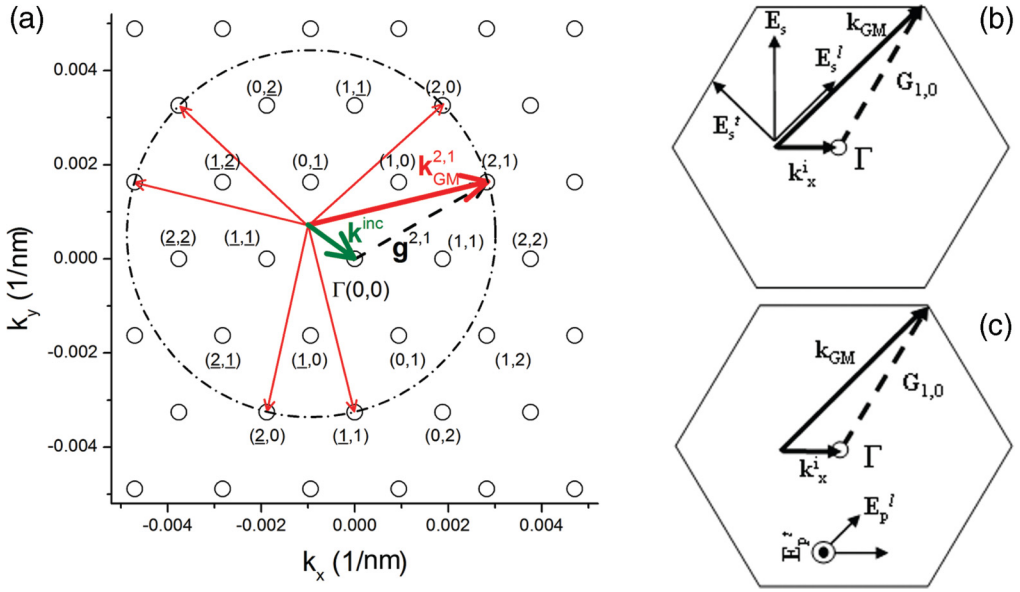

FIG. 6. (Color online) (a) Reciprocal lattice of a 2D hexagonal array of spheres. Numbers indicate the lattice sites. Dashed line is the projection of the Ewald sphere. Thin arrows show the diffraction orders of the incident wave. (b), (c) Sketches of in-plane diffraction orders with transverse and longitudinal orientation of the electric field for s- and p-polarized guided modes, respectively. $\mathbf{E}^{t,l}_{s,p}$ is the vector of the electric field, indices s and p indicate the polarization of the incident light, and indices t and l distinguish between transverse and longitudinal orientation of this vector, respectively. Γ is the center of the Brillouin zone. $\mathbf{G}^{i,k}$ are vectors of the reciprocal lattice. $\mathbf{k}^{\text{inc}}$ and $\mathbf{k}^{i,k}_{\text{GM}}$ are the in-plane projection of the wavevector of incident light and the wavevector of diffracted light, respectively.

that no absorption occurs in a sphere. The electric field of the back-scattered wave can be written in the far field as $\mathbf{E} = (1 + \mathbf{R})\,\mathbf{E}_s$, whereas the electric field of the forward-scattered wave and that transmitted into the substrate can be expressed as $\mathbf{E} = \mathbf{T}\mathbf{E}_s$. Here, $\mathbf{T}$ denotes a matrix representation of a transmission operator suggested in Arnoldus (2005).[28] A sufficiently large number of multipoles was used to ensure the simulation convergence. The dielectric constant of gold was adopted from the *Handbook of Optical Materials*.[29] The scattering geometry was fitted to the layout of experiment that was used to acquire angle-resolved transmission and reflectance spectra.

In the case of a sphere-on-glass configuration, the forward-scattered light intensity is 10 times higher compared with the case of back-scattered light. These spectra contain multipole Mie resonances, which become noticeable only at $\lambda < 800$ nm [Fig. 2(c), curves 8, 9]. The average level of scattered light increases with decreasing wavelength. If the substrate is coated by a gold film, the intensity of the forward-scattered light becomes lower, but the intensity of back-scattered light increases by a factor of 10–40 [Fig. 2(d), curves 12, 13]. Depending on the wavelength, sphere diameter, and the RI of a substrate, the presence of the substrate can either enhance or suppress Mie resonances.[30] In our case, Mie resonances in sphere-Au-glass appear in counterphase to these resonances in the sphere-glass case, and their magnitude is strongly enhanced.

It is instructive to mention that at wavelength less than 1000 nm, the resonances in experimental spectra of the ML-Au-glass hybrid [Fig. 2(b)] show almost the same spacing as Mie resonances of a sphere on a metal substrate [Fig. 2(d)]. Hence, the origin of short-wavelength transmission/reflectance resonances of the ML-Au-glass hybrid is the Mie resonances of individual spheres composing a ML.

The calculated maps of backward- and forward-scattered light for sphere-on-metal show the complex angle dependence of the scattered light intensity (Fig. 7). Naturally, the major Mie resonances possess no angle dispersion. But their intensities are modulated according to the radial distribution of multipole scattering diagrams. Moreover, the intensity of scattered light demonstrates the polarization anisotropy, which affects the resolution of scattering lobes. It is worth noting that the angle distribution of transmitted/reflected light in a ML-Au-glass hybrid may not follow the angle distribution of intensity scattered by a single sphere because of in-plane hybridization of individual resonance states in a close-packed ensemble.

VII. REFLECTANCE AND TRANSMISSION MAPS

Our observations are summarized by plotting transmission maps of the ML-glass sample together with reflectance and transmission maps of the ML-Au-glass sample. In the ML-glass sample, the Fabry–Perot resonance, which corresponds to mode 0, occurs at $\lambda_{\text{FP0}} = 2n_{\text{eff ML}}D \approx 2840$ nm for normal incidence, in which $n_{\text{eff ML}} \approx 1.335$ and $D = 1063$ nm are the effective refractive index and the thickness of ML (i.e., it falls out of the examined spectral range), respectively. In agreement with the transmission of the 50L structure, the Fabry–Perot oscillations can hardly be traced in spectra of the ML-glass sample [Figs. 8(a) and 8(b)] because they are weak and broad compared with diffraction orders of waveguiding modes. The estimate of the onset of diffractively coupled bands in the ML-glass sample is $\lambda_{\text{GM}} = n_{\text{eff ML}}\ D \approx 1335$ nm,[22] for normal light incidence. At shorter wavelengths, a high number

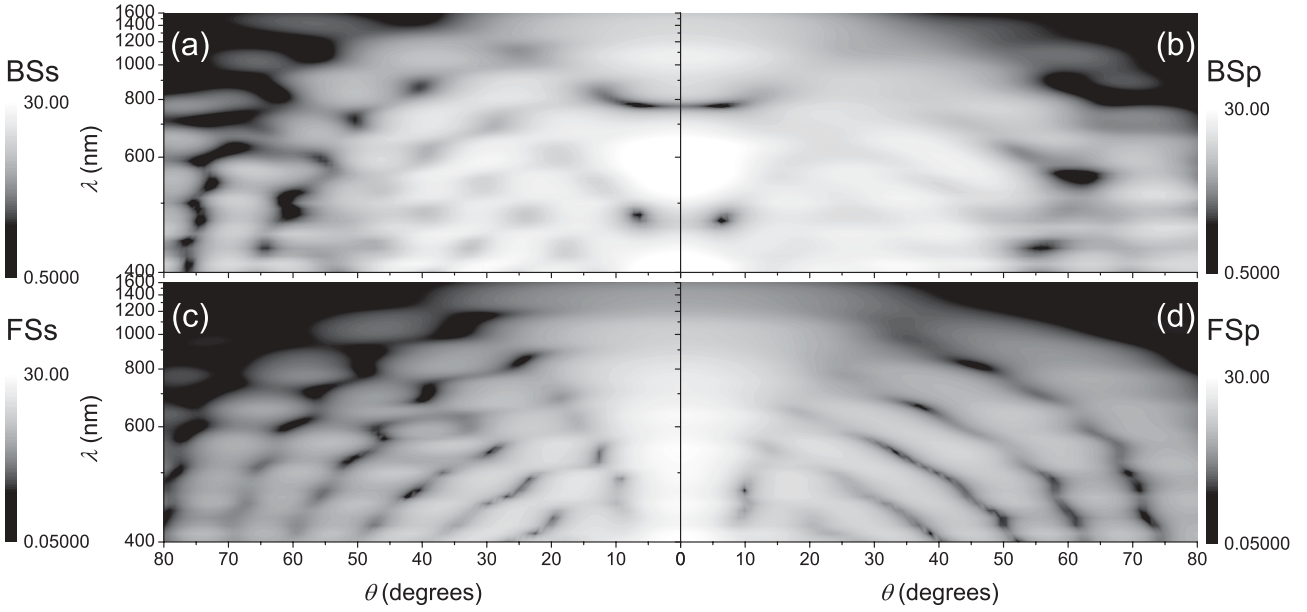

FIG. 7. Calculated maps of (a), (b) backward- and (c), (d) forward-scattered light intensity in *ss*- (left column) and *pp*- (right column) polarized light for the 1063-nm PS sphere on the glass substrate coated with 30-nm Au film.

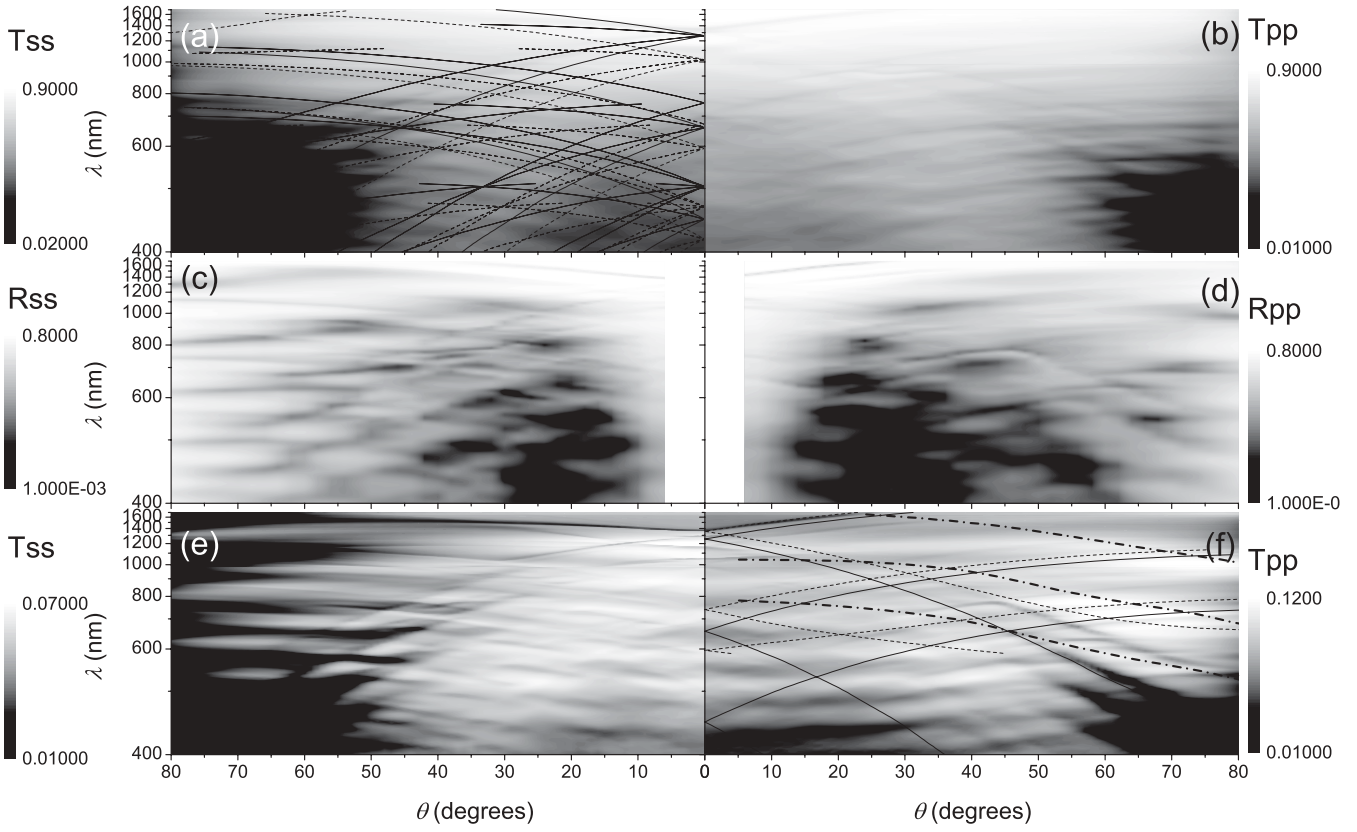

FIG. 8. Experimental maps of (a), (b) transmission of the ML-glass sample and (c), (d) reflectance and (e), (f) transmission of the ML-Au-glass hybrid. Left and right columns are for *ss*- and *pp*-polarized light, respectively. Intensities are plotted on a logarithmic scale. Thin solid and dashed lines in panel (a) show the dispersions of diffraction bands of 0_s and 1_s localized modes, respectively. Solid and dashed lines in panel (f) show the dispersions of diffraction bands of SPP_{ML} and SPP_{sub} modes, respectively. Thick dash-dotted lines show the Fabry–Perot modes 0_p, 1_p, and 2_p of the 50L-Au-glass structure.

of diffraction orders are available for coupling according to the momentum conservation law. To give an example, the transmission map in s-polarized light is overlaid with dispersions of $\mathbf{G}^{-3,-3} \div \mathbf{G}^{3,3}$ diffraction orders originating from 0_s and 1_s guided modes [Fig. 6(a)].

For the ML-Au-glass sample at long wavelengths, the reflectance/transmission maps are dominated by diffraction orders of localized modes [Figs. 8(c)–8(f)]. The dispersions of these modes satisfy the momentum conservation law, as demonstrated by dispersion curves in Fig. 8(f). However, along the wavelength decrease, the contribution of these resonances vanishes. These diffraction bands are conveniently associated with bandlike energy transport in the plane of the sphere lattice.

The Fabry–Perot modes can be recognized by their angle dispersion. According to the 50L-Au-glass waveguide model, the broad Fabry–Perot oscillations become well resolved at high angles of light incidence [dash-dotted lines in Fig. 8(f)]. The positions, dispersions, and magnitudes of Fabry–Perot oscillations in experimental spectra are in remarkable agreement with the Fabry–Perot modes of this model structure (Figs. 5(c)–5(f)].

As was argued above, the multipole Mie resonances overlay the diffraction bands in the mid-spectral range of reflectance and transmission maps and dominate at the short wavelength side of these maps. Unexpectedly, the appearance of Mie resonances in reflectance spectra of the ML-Au-glass sample [Figs. 8(c) and 8(d)] closely resembles the calculated backscattering spectra of the sphere-Au-glass structure [Figs. 7(a) and 7(b)]. In particular, one can distinguish not only the multipole resonances of the sphere but also the radial modulation of the scattering efficiency of these resonances, which is inherited from the scattering of a single sphere. In contrast to the case of a single sphere, the angle-dependent modulation of multipole resonances in experimental maps vanishes at incidence angles of $\theta > 60^\circ$. This observation can be interpreted as evidence of hybridization of resonances of adjacent spheres.

In transmission maps of ML-Au-glass, the multipole Mie resonances are also clearly seen, but the radial modulation of their intensities is hardly detectable [Figs. 8(e) and 8(f)], which makes a difference with calculated forward-scattering spectra of a sphere-on-Au-glass structure [Figs. 7(c) and 7(d)]. In fact, in p-polarized light at $\theta < 35^\circ$ the transmission maxima related to multipole resonances appear almost angle-independent. Apparently, this is a collective effect, which reveals the complex interference of transmitted and reflected waves in the ML-Au-glass architecture.

Owing to close packing of spheres in a ML, the cross-sections of multipole Mie resonance states efficiently overlap each other, but the interaction is not strong enough to hybridize them into a continuous band structure. However, this coupling can facilitate the hoppinglike type propagation of the optical excitation in the plane of the waveguide. In this case, the adequate description can be achieved in terms of the energy transfer between coupled resonators. Thus, hopping transport combines the long interaction time of the light with a spherical resonator and the slow drift of this excitation across the ML. Judging from the similar magnitude of diffractive and Mie resonances, one can derive that both mechanisms can guide approximately the same energy flux along the ML plane.

Obviously, these two transport mechanisms are not independent of each other, since particle scattering is able to couple light to a localized guided mode and, vice versa, scattering of a guided mode at lattice defects can excite localized sphere resonances. In fact, the balance between bandlike and hopping propagation of energy depends on the wavelength. Along the wavelength decrease, the bandlike transport of electromagnetic energy becomes more vulnerable with respect to scattering at lattice defects. At the same time, Mie resonances become more strongly localized and less susceptive to hybridization. Eventually, the hopping transport also will be suppressed, but this may happen in a different spectral range compared with suppression of the eigenmode transport.

VIII. SUMMARY

We demonstrated that turning a 2D slab PhC into a hybrid metal-dielectric plasmonic-photonic crystal can be accomplished by assembling a ML of spheres on a semitransparent flat metal film. The major reason for the resulting strong modification of the ML optical response is the stronger light confinement in a PhC and the generation of diffractively coupled surface plasmon polaritons. We interpreted the optical response of the ML-Au-glass hybrid as the superposition of diffractively coupled guided modes, Fabry–Perot resonances, and multipole Mie resonances. Based on these observations, we assumed that the light propagation in a plane of a hybrid 2D slab PhC is supported by two transport mechanisms: (i) the waveguiding provided by diffractively coupled eigenmodes of a PhC in the spectral range $D/\lambda < 1$ and (ii) the hopping of light coupled to Mie resonances from sphere to sphere in the range $D/\lambda > 1$. In the intermediate range, both mechanisms cooperate in the in-plane light transfer.

It is reasonable to expect that light-matter interaction is enhanced if light is coupled to long-living Mie resonances, compared with light coupled to ballistically propagating modes. Keeping in mind the same confinement strength for both excitations, one would expect that devices operating with coupled localized modes can outperform current prototype light sources and gas sensors based on diffractive modes. Further experiments aimed at examination of this idea in the field of prospective plasmonic-photonic waveguides[31] and thin film solar cells are necessary to validate the assumption concerning stronger light-matter interaction achievable with localized modes.

ACKNOWLEDGMENTS

This work was supported by the German Research Foundation (DFG) Cluster of Excellence "Engineering of Advanced Materials." We thank Gabriele Schäfer for providing us with the PS spheres. NV acknowledges financial support by the Material Science Department of the Mainz graduate school.

*Corresponding author: sergei.romanov@mpl.mpg.de

[1] J. D. Joannopoulos, S. G. Johnson, Jo. N. Winn, and R. D. Meade, *Photonic Crystals: Molding theFlow of Light* (Princeton University Press, Princeton and Oxford, 2008).
[2] E. Lidorikis, M. M. Sigalas, E. N. Economou, and C. M. Soukoulis, Phys. Rev. Lett. **81**, 1405 (1998).
[3] P. D. García, R. Sapienza, J. Bertolotti, M. D. Martín, Á. Blanco, A. Altube, L. Viña, D. S. Wiersma, and C. López, Phys. Rev. A **78**, 023823 (2008).
[4] S. G. Romanov, S. Orlov, A. V. Korovin, O. Zhuromskyy, N. Vogel, K. Landfester, C. K. Weiss, and U. Peschel, Proc. SPIE **8425**, 842550V-1-12 (2012).
[5] M. I. Antonoyiannakis and J. B. Pendry, Europhys. Lett. **40**, 613 (1997).
[6] S. Wedge, I. R. Hooper, I. Sage, and W. L. Barnes, Phys. Rev. B **69**, 245418 (2004).
[7] N. Stefanou, V. Yannopapas, and A. Modino, Comput. Phys. Commun. **113**, 49 (1998).
[8] S. G. Romanov, H. M. Yates, M. E. Pemble, and R. M. De La Rue, J. Phys.: Condens. Matter **12**, 8221 (2000).
[9] E. Istrate and E. H. Sargent, Rev. Mod. Phys. **78**, 455 (2006).
[10] A. L. Yablonskii, E. A. Muljarov, N. A. Gippius, S. G. Tikhodeev, and T. Ishihara, Phys. Status Solidi A **190**, 413 (2002).
[11] S. G. Romanov, A. Regensburger, A. V. Korovin, and U. Peschel, Adv. Mater. **23**, 2515 (2011).
[12] C. D. Dushkin, K. Nagayama, T. Miwa, and P. A. Kralchevsky, Langmuir **9**, 3695 (1993).
[13] B. Ding, M. E. Pemble, A. V. Korovin, U. Peschel, and S. G. Romanov, Phys. Rev. B **82**, 035119 (2010).
[14] L. Shi, X. Liu, H. Yina, and J. Zi, Phys. Lett. A **374**, 1059 (2010).
[15] X. Yu, L. Shi, D. Han, J. Zi, and P. V. Braun, Adv. Funct. Mater. **20**, 1910 (2010).
[16] M. Lopez-Garcıa, J. F. Galisteo-Lopez, A. Blanco, J. Sanchez-Marcos, C. Lopez, and A. Garcıa-Martın, Small **6**, 1757 (2010).
[17] L. Landström, D. Brodoceanu, D. Bauerle, F. J. Garcia-Vidal, S. G. Rodrigo, and L. Martin-Moreno, Opt. Express **17**, 761 (2009).
[18] R. M. Cole, Y. Sugawara, J. J. Baumberg, S. Mahajan, M. Abdelsalam, and P. N. Bartlett, Phys. Rev. Lett. **97**, 137401 (2006).
[19] M. Inoue, Phys. Rev. B **36**, 2852 (1987).
[20] K. Ohtaka, H. Miyazaki, and T. Ueta, Mater. Sci. Eng. B **48**, 153 (1997).
[21] Y. Kurokawa, H. Miyazaki, and Y. Jimba, Phys. Rev. B **69**, 155117 (2004).
[22] S. M. Weekes, F. Y. Ogrin, W. A. Murray, and P. S. Keatley, Langmuir **23**, 1057 (2007).
[23] N. Vogel, L. de Viguerie, U. Jonas, C. K. Weiss, and K. Landfester, Adv. Funct. Mater. **21**, 3064 (2011).
[24] J. Nikoma, R. Loudon, and D. R. Tilley, J. Phys. C **7**, 3547 (1974).
[25] B. K. Vainshtein, V. M. Fridkin, and V. L. Indenbom, *Structure of Crystals*, 3rd ed., Modern Crystallography Series, Vol. 2 (Springer, Berlin, 2000), p. 520.
[26] P. A. Bobbert and J. Vlieger, Physica A **137**, 209 (1986).
[27] E. Fucile, P. Denti, F. Borghese, R. Saija, and O. I. Sindoni, J. Opt. Soc. Am. A **14**, 1505 (1997).
[28] H. F. Arnoldus, J. Opt. Soc. Am. A **22**, 190 (2005).
[29] M. J. Weber, *Handbook of Optical Materials* (CRC Press, Boca Raton, FL, 2003), p. 536.
[30] F. Borghese, P. Denti, R. Saija, E. Fucile, and O. I. Sindoni, Appl. Opt. **36**, 4226 (1997).
[31] S. G. Romanov, A. V. Korovin, M. R. Bahrami, and U. Peschel, Proc. SPIE **8425**, 842514 (2012).